Canadian Science Publishing | Canadian Journal of Chemistry

Exploring Electrochemiluminescence Behaviours and Absolute Quantum Efficiencies of Substituted Metal-Free Phthalocyanine and Unsubstituted Zinc Phthalocyanine

Journal:	*Canadian Journal of Chemistry*
Manuscript ID	cjc-2025-0169.R1
Manuscript Type:	Research Article
Date Submitted by the Author:	29-Aug-2025
Complete List of Authors:	Winslade, Jessica E; Western University, Department of Chemistry Ding, Zhifeng; Western University, Department of Chemistry
Is the manuscript for consideration in a Special Issue or Collection?:	ISESS 2024
Keyword:	Electrochemiluminescence, spectroelectrochemistry, spooling ECL spectroscopy, absolute quantum efficiency, phthalocyanines

Exploring Electrochemiluminescence Behaviours and Absolute Quantum Efficiencies of Substituted Metal-Free Phthalocyanine and Unsubstituted Zinc Phthalocyanine

Jessica E. M. Winslade and Zhifeng Ding*

Department of Chemistry, Western University, London ON N6A 5B7, Canada

*Corresponding author: zfding@uwo.ca (Z.D.)

Abstract

The electrochemiluminescence (ECL) properties and absolute quantum efficiencies (Φ_{ECL}) of octabutoxy-substituted metal-free phthalocyanine ($H_2Pc(\alpha\text{-}OC_4H_9)_8$) and unsubstituted zinc phthalocyanine (ZnPc) were systematically investigated using spectroelectrochemical and photoelectrochemical techniques. $H_2Pc(\alpha\text{-}OC_4H_9)_8$ exhibited negligible ECL in the annihilation pathway but showed a substantial increase in emission with the addition of benzoyl peroxide (BPO), resulting in an Φ_{ECL} of 0.00075 ± 0.00003%. Spectroscopy revealed Q-band transitions at 635 and 780 nm along with the formation of an exciplex at 880 nm in the coreactant ECL system, and a excimer emission at 900 nm were observed via PL. ZnPc demonstrated enhanced ECL with BPO, producing an exciplex emission at 775 nm and an Φ_{ECL} of 0.0099 ± 0.0001%, which is lower than that of $Ru(bpy)_3^{2+}$ but exceeds that of related porphyrin derivatives. These results highlight the ECL behaviours of phthalocyanines and provide insight into their use as ECL luminophores.

Keywords: Electrochemiluminescence, phthalocyanines, absolute quantum efficiency, spectroelectrochemistry, exciplex and excimer, spooling ECL spectroscopy

Introduction

Electrochemiluminescence (ECL) is a process in which light is emitted as a result of an excited-state species being produced from high-energy electron transfer reactions between electrogenerated radical species and relaxing to its ground state.[1-3] In parallel to electrochemical detections,[4] ECL has become a valuable tool in analytical chemistry, medical diagnostics and chemical assays due its high sensitivity, spatiotemporal control, and background-free detection.[2, 5] The study of ECL-active luminophores is essential for advancing applications in sensing, light-

emitting devices, and molecular electronics. However, beside research on ECL of metal complexes,[6-8] investigations on phthalocyanines remain under-researched while they have been extensively studied in photophysical and electrochemical contexts.[9-11]

In particular, metal-free and metalated phthalocyanines offer distinct electronic structures that influence their luminescent behaviour. 1,4,8,11,15,18,22,25-octa-n-butoxyphthalocyanine ($H_2Pc(\alpha\text{-}OC_4H_9)_8$) presents enhanced solubility and disrupted aggregation due to its bulky peripheral alkoxy groups, while unsubstituted zinc phthalocyanine (ZnPc) serves a structurally simpler, planar comparison. Investigating how these structural differences affect ECL behaviour and absolute ECL quantum efficiency provides insight into the use of phthalocyanines as electrochemiluminescent luminophores.

In this work, we systematically study and compare the ECL properties and absolute quantum efficiencies (Φ_{ECL}) of $H_2Pc(\alpha\text{-}OC_4H_9)_8$ and ZnPc under annihilation and coreactant pathways. The electrochemistry and electrochemiluminescence of $H_2Pc(\alpha\text{-}OC_4H_9)_8$ and ZnPc were conducted to provide insight into the fundamental photophysical processes governing their electrochemiluminescence. Φ_{ECL} enables a rigorous comparison of light-emitting performance across different excitation methods and compounds. This study highlights the ECL behaviour of phthalocyanine systems and provides fundamental insights to contribute to broader understanding of phthalocyanines as potential emitters in optoelectronic applications, biosensing, and bioimaging.

Experimental

Chemicals

Tetrabutylammonium perchlorate (TBAP, for electrochemical analysis, ≥ 99.0%), dimethyl sulfoxide (DMSO, anhydrous (Sure Seal®, ≥99.9%), dichloromethane (DCM, anhydrous (Sure Seal®), ≥ 99.8%, contains 40-150 ppm amylene as stabilizer), benzoyl peroxide (BPO, reagent grade, 97%), ferrocene (Fc, 98%), 1,4,8,11,15,18,22,25-octabutoxy-29*H*,31*H*-phthalocyanine ($H_2Pc(\alpha\text{-}OC_4H_9)_8$, **Figure 1A**), dye content 95%), and zinc phthalocyanine (ZnPc, dye content 97%, **Figure 1B**) were all purchased from Sigma-Aldrich Canada (Mississauga, ON) and stored under inert atmosphere.

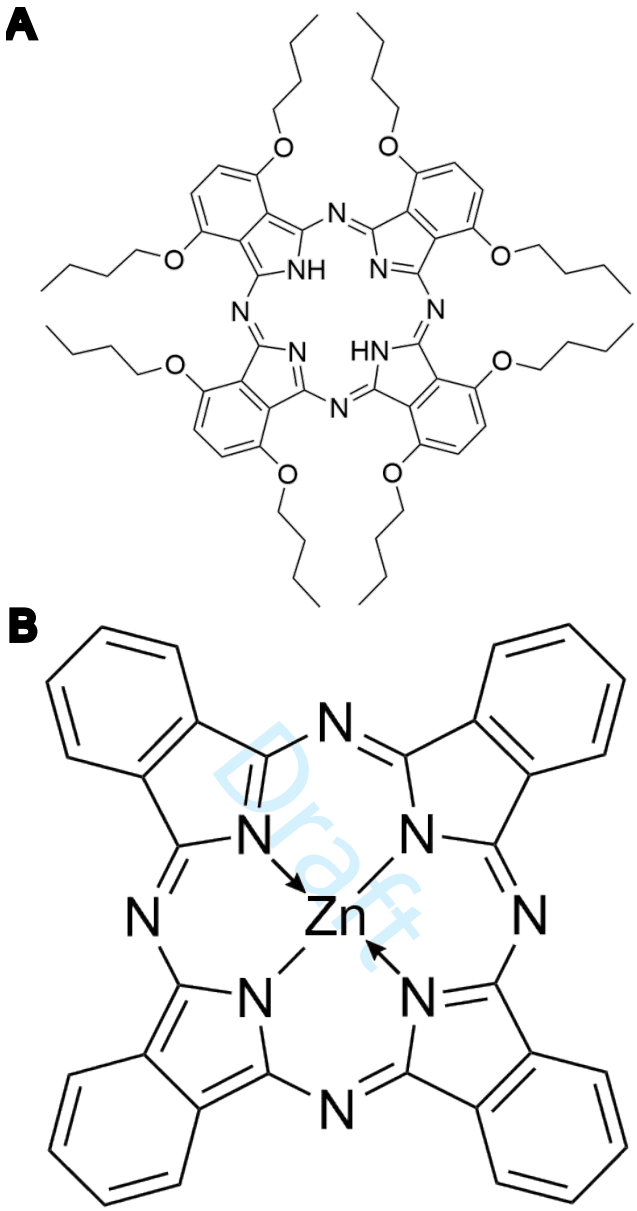

Figure 1. Chemical structures of (A) 1,4,8,11,15,18,22,25-octabutoxy-29*H*,31*H*-phthalocyanine ($H_2Pc(\alpha\text{-}OC_4H_9)_8$), and (B) unsubstituted zinc phthalocyanine (ZnPc).

Instrumentation

A custom-designed photoelectrochemical cell was used for all electrochemistry and ECL measurements.[12] The cell was equipped with a Pt disk working electrode (2 mm diameter), a Pt coil counter electrode, and a Pt coil quasi-reference electrode. The bottom of the cell features a

flat Pyrex window to enable light detection from the working electrode. Electrolyte solutions of 0.1 mM $H_2Pc(\alpha\text{-}OC_4H_9)_8$ were prepared with 0.1 M TBAP as the supporting electrolyte in 4 mL DCM as the solvent. ZnPc electrochemical solutions were prepared similarly, using 0.025 mM ZnPc, 0.1 M TBAP as the supporting electrolyte, and 4 mL DMSO as the solvent. PL solutions were prepared by diluting 500 µL of the respective electrochemical solution in 3 mL of the corresponding solvent. The airtight ECL cell was assembled inside a nitrogen-atmosphere glovebox (Model Nexus I, Vacuum Atmospheres Company, Hawthorne, CA) to maintain an environment with minimal oxygen and moisture.

Differential pulse voltammograms (DPVs) were recorded using an Autolab electrochemical workstation (Model PGSTAT302N, Metrohm BV, Switzerland). The DPV parameters were as follows: 0.005 V step potential, 0.025 V pulse amplitude, 0.05 s step width. Potential pulsing experiments consisted of widths of 1 s (0.5 Hz), 0.5 s (1 Hz), 0.1 s (5 Hz), and 0.05 s (10 Hz). Cyclic voltammogram (CV) scans were performed using the same electrochemical setup at a scan rate of 100 mV/s. Fc was added at the end of each experiment as an internal standard to calibrate the electrochemical potential window. The formal redox potential of the Fc/Fc^+ couple was taken to be 0.342 V vs. the saturated calomel electrode (SCE).[13-15]

ECL-voltage curves were recorded using the electrochemical workstation coupled with a photomultiplier tube (PMT, R928P, Hamamatsu, Japan) held at −750 V using a high-voltage power supply. ECL emitted in the vicinity of the working electrode was collected by the PMT through the flat Pyrex window at the bottom of the cell. The photocurrent collected by the PMT was converted into a photovoltage signal using a picoammeter (Model 487, Keithley, Cleveland, Ohio). The resulting signal was simultaneously sent to one of the two auxiliary channels of the

Autolab electrochemical setup, enabling the generation and recording of ECL-voltage curves using the Metrohm Nova software.

ECL spectra were measured using a potential program applied by an electrochemical workstation (CHI 610A, CH Instruments, Austin, Texas). ECL emission was collected through the Pyrex window of the cell and directed into a spectrograph (Teledyne Princeton Instruments Acton 2300i, Trenton, New Jersey), where it was dispersed by a grating of 50 l/mm blazed at 600 nm. The output was recorded on a back-illuminated charge-coupled device (CCD) camera (DU401-BR-DD-352, Andor Technology, UK),[12] which was electrothermally cooled to −65 °C. Before all spectra acquisition, a mercury-argon light source (HG-1, Ocean Insight, Orlando, Florida) was used to calibrate the wavelengths.

Spectroelectrochemistry was conducted using a thin layer quartz glass spectroelectrochemical cell (Gaoss Union (TianJin) Photoelectric technology co. LTD, China) equipped with a Pt Gauze working electrode, Pt counter electrode, Pt quasi-reference electrode, and Teflon cap. A 532 nm diode-pumped laser (Verdi™ V-5, Coherent Inc., Santa Clara, CA) beam was directed through the quartz cell using an optical fibre cable, providing a stable and intense monochromatic light source, with the laser power set to 0.01 W. The lithium triborate (LBO) crystal temperature was controlled by a resistive heater, ensuring the LBO crystal is held at a temperature of approximately 150°C. A potential profile was applied to the solution using a CHI 610A electrochemical workstation while the spectroscopy was recorded on the set of the back-illuminated CCD camera and Acton 2300i spectrograph as in the measurement of ECL spectroscopy.[16]

Photoluminescence data was recorded in a similar fashion to spectroelectrochemistry results, using the CCD camera and spectrograph set. A four-sided translucent thin layer quartz

glass cell with a screw cap (Type 41 cuvette, FireflySci Canada, Ottawa, Canada) was assembled in the glovebox, similarly to the ECL solutions as described above.

The ECL signal measured as photocurrent on a calibrated PMT during an electrochemical process was converted the absolute number of emitted photons at each wavelength in considerations of the measurement environment, a necessary step for determining the absolute ECL quantum efficiency (Φ_{ECL}). Detailed experimental procedures and absolute irradiance information along with a custom-made Matlab code have been presented elsewhere.[17-18] The total charge was determined by integrating the Faradaic current over the experiment duration, as shown in **Equation 1**. Using the elementary charge constant (e), the total charge was converted to the number of injected electrons, as shown in **Equation 2**. Finally, Φ_{ECL} of the system was determined using **Equation 3**.

(1) $$\text{Total charge} = \int_a^b \text{current}\, dt$$

(2) $$\text{Total electrons} = \frac{\text{Total charge}}{e}$$

(3) $$\phi_{ECL} = \frac{\text{Total photons}}{\text{Total electrons}} \times 100\%$$

Results and Discussion

Electrochemistry and Electrochemiluminescence of $H_2Pc(\alpha\text{-}OC_4H_9)_8$

Figure 2A shows the DPVs of 0.1 mM $H_2Pc(\alpha\text{-}OC_4H_9)_8$ at a 2 mm diameter platinum electrode in a 0.1 M TBAP DCM electrolyte solution, with arrows indicating the direction of

scan. Two reduction reactions and two oxidation waves were observed within the electrochemical window of DCM. Radical anions ($H_2Pc(\alpha\text{-}OC_4H_9)_8^{\bullet-}$) and dianions ($H_2Pc(\alpha\text{-}OC_4H_9)_8^{2-}$) are produced via two quasi-reversible electrochemical reduction reactions (**Equations 4-5**) at formal potentials of −1.06 V and −1.47 V vs. SCE, respectively. Additionally, radical cations ($H_2Pc(\alpha\text{-}OC_4H_9)_8^{\bullet+}$) and dications ($H_2Pc(\alpha\text{-}OC_4H_9)_8^{2+}$) are produced at formal potentials of +0.28 V and +0.51 V vs. SCE, respectively, during two quasi-reversible oxidation reactions (**Equations 6-7**). Our data correlates well with the electrochemical redox potentials of similarly substituted metal-free phthalocyanine compounds reported by Atif Koca.[10]

(4) $$H_2Pc(\alpha\text{-}OC_4H_9)_8 + e^- \rightarrow H_2Pc(\alpha\text{-}OC_4H_9)_8^{\bullet-}$$

(5) $$H_2Pc(\alpha\text{-}OC_4H_9)_8^{\bullet-} + e^- \rightarrow H_2Pc(\alpha\text{-}OC_4H_9)_8^{2-}$$

(6) $$H_2Pc(\alpha\text{-}OC_4H_9)_8 \rightarrow H_2Pc(\alpha\text{-}OC_4H_9)_8^{\bullet+} + e^-$$

(7) $$H_2Pc(\alpha\text{-}OC_4H_9)_8^{\bullet+} \rightarrow H_2Pc(\alpha\text{-}OC_4H_9)_8^{2+} + e^-$$

(8) $$H_2Pc(\alpha\text{-}OC_4H_9)_8^{\bullet-} + H_2Pc(\alpha\text{-}OC_4H_9)_8^{\bullet+} \rightarrow H_2Pc(\alpha\text{-}OC_4H_9)_8 + H_2Pc(\alpha\text{-}OC_4H_9)_8^{*}$$

(9) $$H_2Pc(\alpha\text{-}OC_4H_9)_8^{*} \rightarrow H_2Pc(\alpha\text{-}OC_4H_9)_8 + h\nu$$

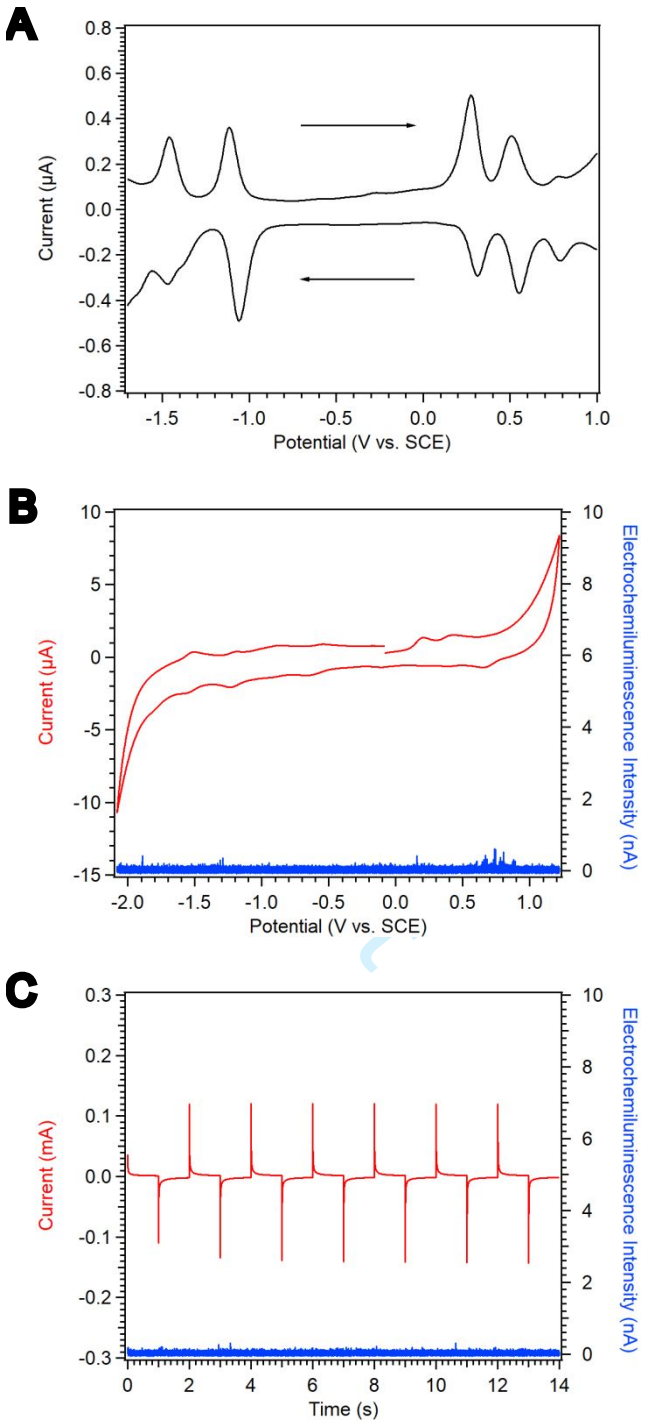

135

136 **Figure 2.** Electrochemical analysis and ECL measurements via the annihilation pathway of 0.1
137 mM $H_2Pc(\alpha\text{-}OC_4H_9)_8$ at a 2 mm diameter platinum working electrode in DCM with 0.1 M TBAP
138 as the supporting electrolyte. Profiles include (A) DPVs, (B) CV (red) and the corresponding

ECL-voltage curve (blue) scanning at a rate of 100 mV/s and cycling between +1.22 V and −2.08 V vs. SCE., and (C) chronoamperogram and ECL-time curve during a potential pulsing experiment at a frequency of 0.5 Hz in a potential range between the first oxidation (+0.50 V vs. SCE) and the first reduction (−0.84 V vs. SCE).

Figure 2B displays the CV (red) and ECL-voltage curve (blue) in the annihilation pathway, in which ECL emission typically arises from the relaxation of $H_2Pc(\alpha\text{-}OC_4H_9)_8^*$, produced via the electron transfer between $H_2Pc(\alpha\text{-}OC_4H_9)_8^{\bullet+}$ and $H_2Pc(\alpha\text{-}OC_4H_9)_8^{\bullet-}$ in the vicinity of the working electrode surface (**Equation 8-9**). No appreciable emission was detected, with the ECL intensity remaining below 0.6 nA. The low ECL emission is attributed to the unstable radical species and their low reactivity, similar to porphyrin ECL studies,[19-20] spectroelectrochemistry of phthalocyanines,[10] and investigations of other ECL compounds.[1-2]

To minimize the time gap between the formation of radical ions, potential pulsing is utilized where a potential profile rapidly switches between the anodic and cathodic regions. **Figure 2C** demonstrates the potential pulsing results between the first oxidation (+0.50 V vs. SCE) and the first reduction (−0.84 V vs. SCE), with the remaining three potential pulsing combinations presented in **Figure S1**. This method enables the electrogeneration of both radical anionic and radical cationic species within a short time window of 100 ms, allowing electron transfer reactions to occur before significant depletion. The current (red) and ECL (blue) curves were recorded simultaneously as a function of time. Notably, only a negligible ECL signal ($\lesssim$ 1.3 nA) was observed in **Figure 2C** and across all other three combinations (**Figure S1**). This is likely due to slow reaction rates of radical species in generating the excited states.

To further improve the ECL of $H_2Pc(\alpha\text{-}OC_4H_9)_8$ a coreactant was added. Due to the instability of phthalocyanine cations shown in the DPVs in **Figure 2A**,[10] benzoyl peroxide was selected as the coreactant species due to its radical anion ($BPO^{\bullet-}$) forming in a similar potential region as $H_2Pc(\alpha\text{-}OC_4H_9)_8$. To better study the ECL properties of the $H_2Pc(\alpha\text{-}OC_4H_9)_8$/BPO system, the ECL-voltage curve was recorded simultaneously with the CV at a scan rate of 100 mV/s, **Figure 3A**. In comparison to the CV of $H_2Pc(\alpha\text{-}OC_4H_9)_8$ in the annihilation pathway (**Figure 2B**), $BPO^{\bullet-}$ is electrogenerated at −1.90 V vs. SCE, **Figure 3A**,[1] within a potential range close to that of the $H_2Pc(\alpha\text{-}OC_4H_9)_8$ radical anions. This process, known as the reduction-oxidative coreactant pathway, utilizes the formation of the strongly oxidizing benzoate radical.[2] Using this strategy, the ECL signal reached an intensity of 1727 nA (**Figure 3A**) — nearly 2200-fold greater than the emission observed in the annihilation pathway. The ECL-voltage curve exhibited an onset at −1.80 V vs. SCE and maxima at −2.30 V vs. SCE. The delay between the onset and maximum ECL-voltage is likely due to the balance between the diffusion and consumption of the reactive species.

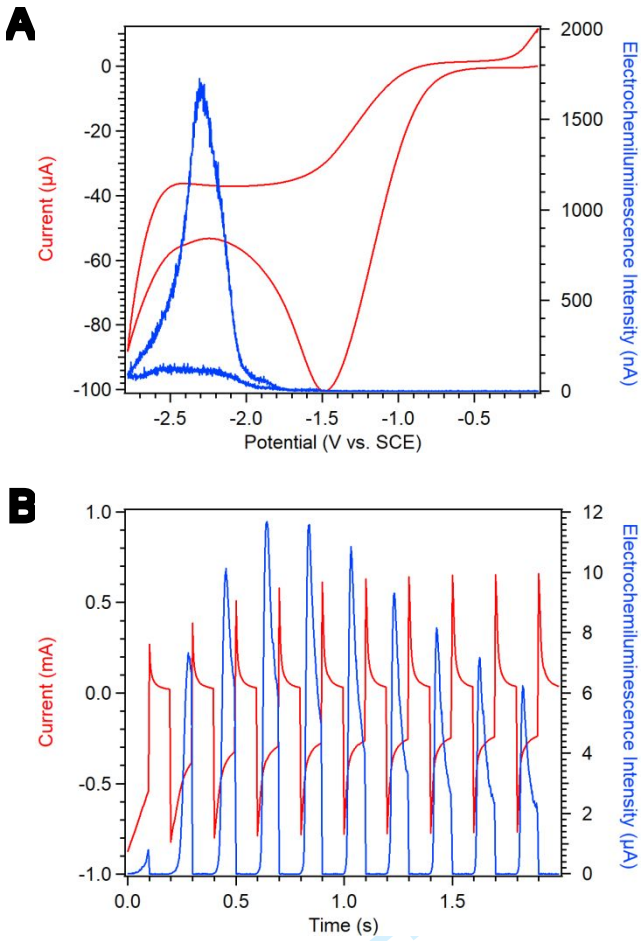

174

175 **Figure 3.** (A) CV (red) and ECL-voltage curve (blue) of 0.1 mM $H_2Pc(\alpha\text{-}OC_4H_9)_8$ and 5 mM
176 BPO in DCM with 0.1 M TBAP solution. A scan rate of 100 mV/s was utilized, cycling between
177 −0.08 V and −2.78 V vs. SCE. (B) The current-time (red) and ECL-time (blue) curves are shown
178 pulsing between potentials of −2.78 V and −0.08 V vs. SCE at a frequency of 5 Hz.

179 By applying potential pulsing, the rapid alternating of potentials enables a greater
180 opportunity for radical species to meet and react for excited state generation before their decay in
181 the vicinity of the working electrode surface, increasing the ECL emission. **Figure 3B** shows the
182 potential pulsing conducted for the $H_2Pc(\alpha\text{-}OC_4H_9)_8$/BPO coreactant system. Potential pulsing
183 was applied at frequencies of 0.5 Hz, 1 Hz, 5 Hz, and 10 Hz. At the slowest frequency, 0.5 Hz,
184 potential steps have a duration of 1 second. By pulsing at a higher frequency, the decreased

potential step duration allows for the reactive radical species to encounter one another before their decay, **Figure 3B**. This is evident when comparing the maximum ECL intensity at various potential pulsing frequencies. Using the potential pulsing technique, the lowest ECL intensity was observed to be 2470 nA at a frequency of 0.5 Hz (1 second potential step duration) in **Figure S2A**, whereas the ECL intensity is higher at higher frequencies, **Figure 3B**. Notably, ECL intensity of 28.6 μA is more than 10-fold greater than the observed signal at 0.5 Hz, at a frequency of 10 Hz (50 milliseconds pulse step) in **Figure S2C**.

Electrochemiluminescence Spectroscopy of $H_2Pc(\alpha\text{-}OC_4H_9)_8$/BPO Coreactant System

To gain insight into the $H_2Pc(\alpha\text{-}OC_4H_9)_8$/BPO ECL emission, spectroscopy analysis was conducted. This enabled the collection of wavelength-resolved emission data, allowing for the characterization of the emitted light during electrochemical stimulation.

Figure 4A shows the accumulated ECL spectrum obtained during a CV experiment that scanned from −0.08 V to −2.78 V vs. SCE at a scan rate of 100 mV/s. Three peak wavelengths were curve-fitted, with the first being at 635 nm (red), and the second at 780 nm (blue). We believe these are attributed to the Q(0,0) band and its vibronic band Q(0,1) of $H_2Pc(\alpha\text{-}OC_4H_9)_8$, as reported previously on studies of phthalocyanines optical spectroscopy,[21-22] and porphyrin derivative ECL spectroscopy.[19-20, 23] Interestingly, the third peak at 880 nm (orange) was observed. **Figure 4B** shows the photoluminescence spectra of 0.01 mM $H_2Pc(\alpha\text{-}OC_4H_9)_8$ with 0.01 M TBAP in DCM. The solution was excited using a 532 nm laser equipped with a long-pass filter. The resulting peaks were observed at 635 nm, 800 nm, correlating with previously reported fluorescence of solid metal-free phthalocyanines.[24] The 900 nm peak might be the excimer formation and the ECL emission at 880 nm may be a result of exciplex formation.[25] Importantly, the fluorescence lifetime provides insight into the efficiency and pathway of light

emission. Previously, Kosonocky et al. determined the lifetime of excited singlet-state metal-free phthalocyanines to be ~2.0 ns.[26] Higher concentrations can favour both exciplex and excimer formation; however, at the relatively higher concentration conditions used in ECL, the self-absorption peak is significantly enhanced, reducing the apparent intensity and resolution of the exciplex emission. As a result, the exciplex band in the ECL spectra is less distinguishable compared to the excimer contribution in the PL spectra, where lower concentrations minimize self-absorption effects.[27] Additionally, the ECL intensity reaches 2804 counts (**Figure 4A**), compared to the 24 948 counts and 5430 counts observed in the PL pathways (**Figure 4B** and **Figure S3**), respectively. This difference reflects the generation of excited states via direct photon absorption by a controlled, high-photon flux 532 nm laser beam in the PL process compared to the formation of excited states via bimolecular electron transfer between electrogenerated radical species in the vicinity of the working electrode — a diffusion- and stability-limited process. Notably, the 880 nm peak emission in **Figure S3** has a relatively low intensity relative to the Q(0,0) band at 635 nm which may be a result of BPO being thermally decomposed.

To better understand how the presence of BPO affects the photoluminescence of $H_2Pc(\alpha\text{-}OC_4H_9)_8$, the PL was recorded before and after the addition of BPO using a CCD camera to record emission wavelength and a 532 nm laser with a long-pass filter as the excitation source. Notably, changes were observed in the emission profiles (**Figure 4B** with no BPO and **Figure S3** with BPO), specifically the intensity of the 635 nm and 880 nm peaks. The addition of BPO resulted in an increased intensity of the 635 nm peak, alongside a decrease in the 880 nm peak; the intensity increase at 635 nm may be indicative of an increase in self-absorption. Exciplex and excimer formation is believed to be the 880 nm and 900 nm peaks, respectively, as the

heterogeneous complex of $H_2Pc(\alpha\text{-}OC_4H_9)_8$ and benzoate will have a shorter wavelength, due to the decreased size, in contrast to the homogeneous excimer complex of $H_2Pc(\alpha\text{-}OC_4H_9)_8$ and $H_2Pc(\alpha\text{-}OC_4H_9)_8$.[3, 8, 25, 28-29]

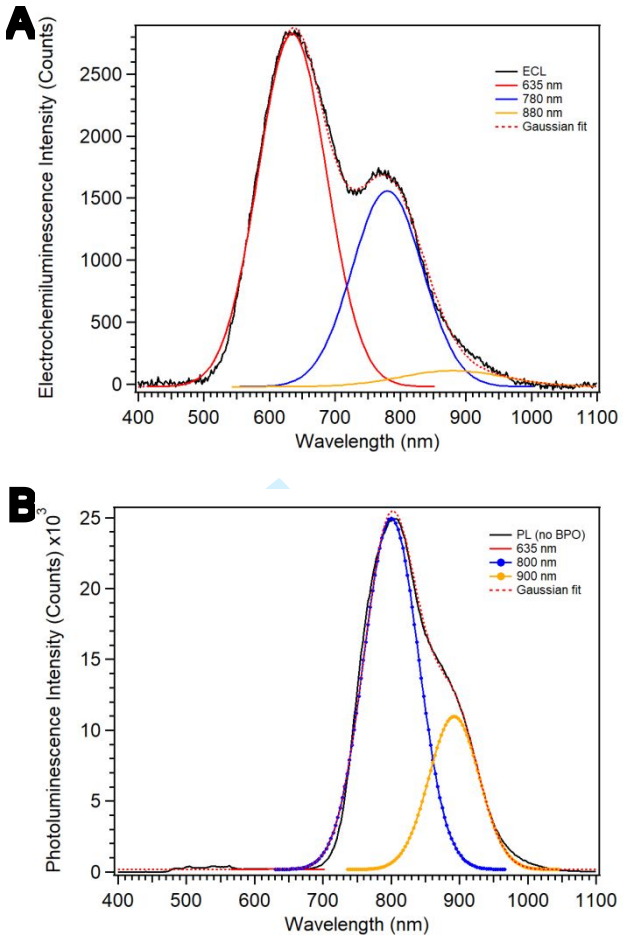

Figure 4. (A) Accumulated ECL intensity of 0.1 mM $H_2Pc(\alpha\text{-}OC_4H_9)_8$ with 5 mM BPO coreactant system during a CV scan cycling from −0.08 V to −2.78 V vs. SCE at a scan rate of 100 mV/s. (B) Photoluminescence of 0.01 mM $H_2Pc(\alpha\text{-}OC_4H_9)_8$ with 0.01 M TBAP excited by a 532 nm laser.

Spooling ECL spectroscopy was utilized to examine the ECL evolution and devolution. **Figure 5A** shows the three-dimensional view of spooling ECL spectroscopy during a CV scan from −0.08 V to −2.78 V vs. SCE at a scan rate of 100 mV/s with a 0.5 second accumulation

time per spectrum. The maximum ECL emission was observed to be at −2.12 V vs. SCE using the ECL intensity vs. potential view from **Figure 5B**, which is similar to the ECL-voltage maximum emission peak, at −2.30 V vs. SCE, observed using the PMT. The evolution of ECL in the cathodic scan began around −1.85 V vs. SCE and its corresponding devolution around −2.20 V vs. SCE, while evolution and devolution in the anodic scan occurred near −2.80 V and −2.45 V vs. SCE, respectively. Using the spooling ECL spectra, we can also better understand the excited states being produced, and how these states may change during the ECL process. The intensity-wavelength profile (**Figure 5C**) developed with a wide peak at a wavelength of 635 nm; as the ECL evolved, the emission peak adjusted, presenting as a narrow peak with an asymmetric broadening toward the longer wavelengths of 780 and 880 nm. The resulting spectra provide key information about the emission profile, including the evolution and devolution of ECL along with the formation and consumption of excited state species. These spectroscopic analyses are critical for better understanding the electrochemiluminescence of phthalocyanines.

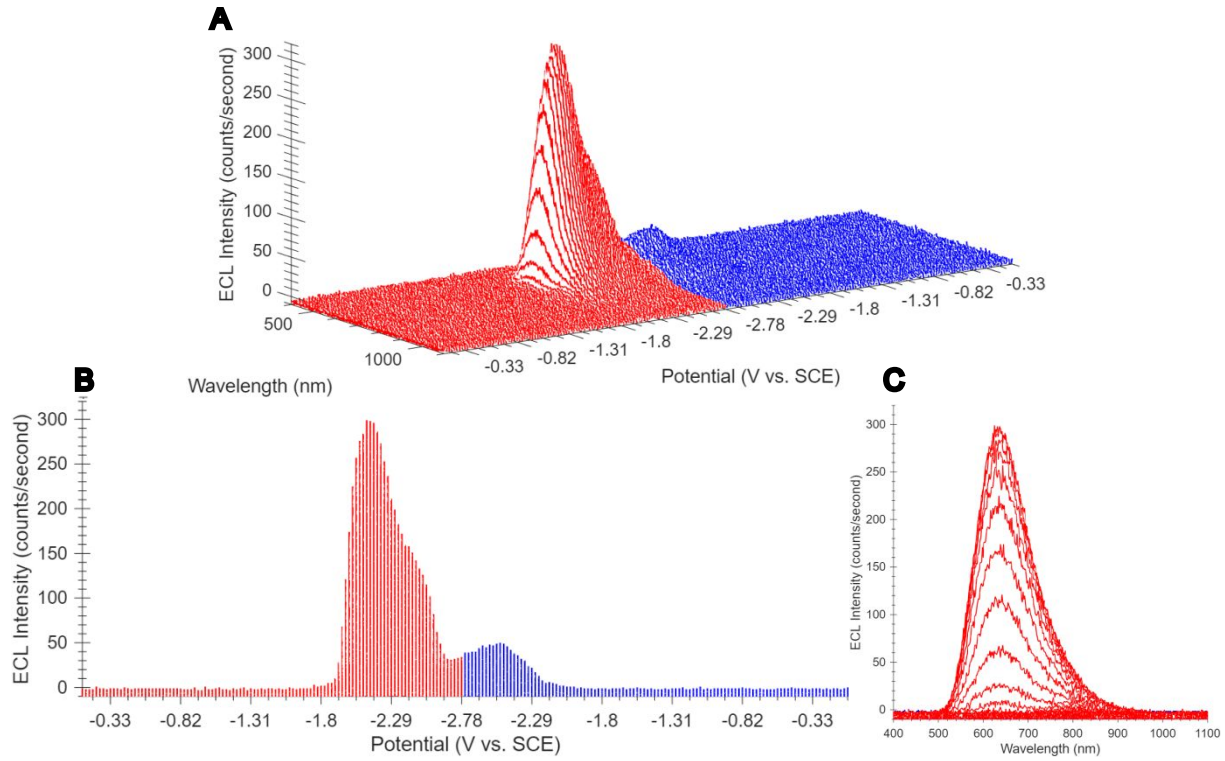

Figure 5. Spooling ECL spectra of 0.1 mM $H_2Pc(\alpha\text{-}OC_4H_9)_8$ with 5 mM BPO in DCM during a CV experiment performed at 100 mV/s where the anodic scan is depicted in red and the cathodic scan in blue. Three views are provided, with (A) being three-dimensional, (B) being ECL intensity vs. potential, and (C) being ECL intensity vs. wavelength.

Using the potential pulsing technique, the highest ECL intensity is 5461 counts at a frequency of 10 Hz (50 milliseconds per pulse, **Figure 6D**), which is more than 5-fold greater than that observed signal at 0.5 Hz. The accumulation spectra shown in **Figures 6A-D** indicate that a faster potential pulsing frequency results in the two radical reactants encountering one another faster, whereas the low pulsing frequency results in a time gap between the generation of these reactive radical species. This indicates that the stability of the reactive radical species plays a dominant role in the magnitude of ECL intensity. Additionally, as the frequency of the pulsing increases, the 635 nm emission peak increases in intensity; this may be indicative of an exciplex formation being favoured at faster reaction conditions.

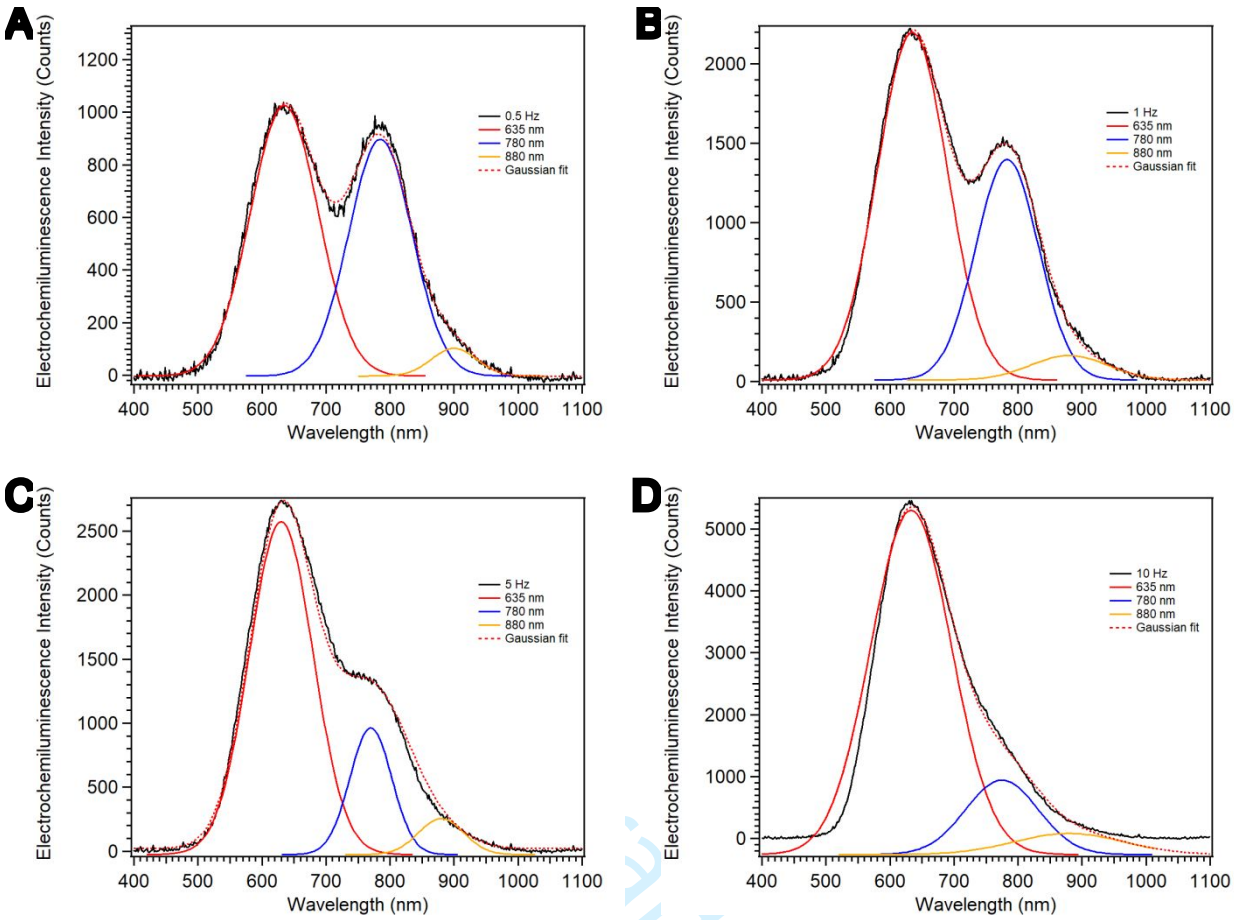

Figure 6. Accumulation spectra of 0.1 mM $H_2Pc(\alpha\text{-}OC_4H_9)_8$ with 0.1 M TBAP and 5 mM BPO in DCM. The potential pulsing technique was used to pulse between potentials of −2.78 V and −0.08 V vs. SCE at frequencies of (A) 0.5 Hz, (B) 1 Hz, (C) 5 Hz, and (D) 10 Hz.

Spectroelectrochemistry of $H_2Pc(\alpha\text{-}OC_4H_9)_8$

Notably, metal-free phthalocyanines can exhibit up to two oxidation states and four reduction states, with characteristic spectroscopic features appearing in the 600-900 nm near-IR region.[10, 24] Previously, spectroelectrochemistry has been useful for observing the formation and decomposition of electrogenerated species; as the oxidation state of a phthalocyanine compound is altered, a corresponding change in the compound's colour may be observed.[10] **Figure S4** shows the spectroelectrochemistry of $H_2Pc(\alpha\text{-}OC_4H_9)_8$ when excited by a 532 nm laser equipped

with a long-pass filter. Cyclic voltammetry was performed by cycling the potential from −2.5 V to +2.5 V vs. Fc/Fc^+ while simultaneously monitoring the emission through spooling spectroscopy, with each scan having a 10 ms accumulation time. Interestingly, we observed the emission peaks were redshifted by approximately 30 nm with respect to the PL (**Figure 4B**). However, this data aligns closely, indicating that the Q(0,0) band is present around 635 nm, its vibronic Q(0,1) band around 800 nm, and the corresponding excimer around 900 nm.

Absolute Electrochemiluminescence Quantum Efficiency of $H_2Pc(\alpha\text{-}OC_4H_9)_8$

Table 1 reports the absolute electrochemiluminescence quantum efficiency of $H_2Pc(\alpha\text{-}OC_4H_9)_8$ in the coreactant pathway using BPO as the oxidative coreactant. Despite the relatively weak emission observed compared to other ECL-active compounds,[18] a Φ_{ECL} value of 0.00075 ± 0.00003% was calculated based on integrated emission intensity, the number of emitted photons, the total charge passed during the reaction. This value is consistent with the structural characteristics of $H_2Pc(\alpha\text{-}OC_4H_9)_8$, which features a metal-free centre and alkoxy peripheral substituents that may promote aggregation, leading to self-quenching of excited states and increased nonradiative decay. Furthermore, the radical intermediates formed from $H_2Pc(\alpha\text{-}OC_4H_9)_8$ may be less stable or less reactive toward BPO-derived radicals, thereby limiting the overall efficiency of the ECL process. Notably, the use of potential pulsing resulted in enhanced absolute ECL quantum efficiency by rapidly regenerating the reactive radical species, increasing the probability of electron transfer reactions occurring. Nonetheless, the measurable 0.00075 ± 0.00003% confirms the ability of substituted metal-free phthalocyanines to engage in coreactant ECL, albeit with lower efficiency compared to its metalated analogue, with Φ_{ECL} values reported in **Table 2**, and other porphyrin derivatives, such as protoporphyrin IX dimethyl ester with a Φ_{ECL} value of 0.0018% reported by Zhan et al.[19]

Table 1. Absolute Electrochemiluminescence Quantum Efficiency of 0.1 mM $H_2Pc(\alpha\text{-}OC_4H_9)_8$ with 5 mM BPO in a DCM solution with 0.1 M of TBAP using various electrochemical techniques.

Technique	Absolute Electrochemiluminescence Quantum Efficiency (%)
Cyclic Voltammetry	0.00035 ± 0.00003
0.5 Hz Potential Pulsing	0.00016 ± 0.00001
1 Hz Potential Pulsing	0.00020 ± 0.00002
5 Hz Potential Pulsing	0.00073 ± 0.00003
10 Hz Potential Pulsing	0.00075 ± 0.00003

Electrochemistry and Electrochemiluminescence of Unsubstituted ZnPc

Figure 7A shows the DPV scans of 0.025 mM ZnPc in a DMSO solution with a supporting electrolyte of 0.1 M TBAP. In the anodic scan, two oxidation states are elucidated, with the radical cation ($ZnPc^{\bullet+}$) being produced at +0.26 V vs. SCE (irreversible, **Equation 10**), and the dication ($ZnPc^{2+}$) being produced +0.62 V vs. SCE (quasi-reversible, **Equation 11**). In the cathodic scan, two quasi-reversible reduction peaks are observed at −0.90 V and −1.42 V vs. SCE (**Equations 12-13**). These peaks correspond to the electrogenerated anionic species of $ZnPc^{\bullet-}$ and $ZnPc^{2-}$, respectively. Additionally, two irreversible reduction peaks are observed at −1.63 V and −1.96 V vs. SCE (**Equations 14-15**).

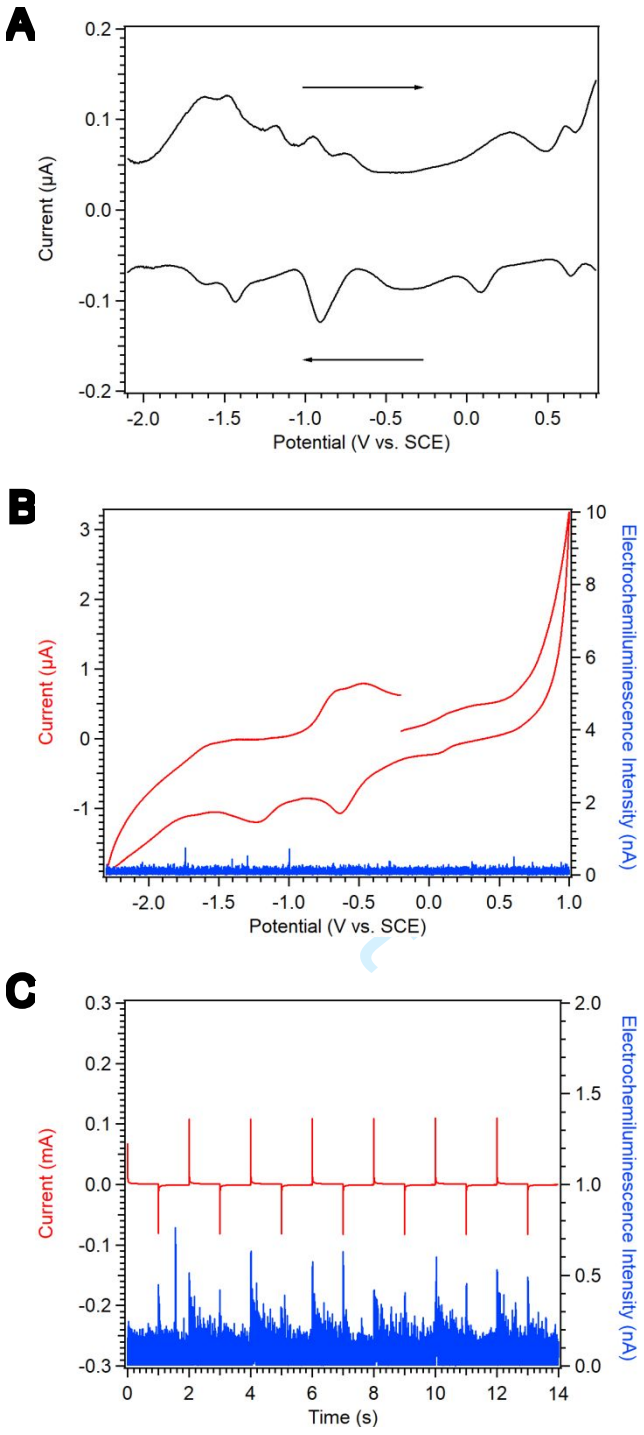

316

317 **Figure 7.** Electrochemical analysis and ECL measurements via the annihilation pathway of
318 0.025 mM ZnPc at a 2 mm diameter platinum working electrode in DMSO with 0.1 M TBAP as
319 the supporting electrolyte. Profiles include (A) DPVs, (B) CV (red) and ECL-voltage curve

(blue) scanning at a rate of 100 mV/s and cycling between +1.00 V and −2.30 V vs. SCE, and (C) potential pulsing at a frequency of 0.5 Hz between the second oxidation (+0.71 V vs. SCE) and the first reduction (−1.07 V vs. SCE).

Figure 7B presents the CV (red) alongside the ECL-voltage profile (blue) for unsubstituted ZnPc in the annihilation pathway. Two quasi-reversible reduction peaks are observed at −0.63 V and −1.21 V vs. SCE, while the other two reduction and two oxidation peaks are not well-resolved. In this electrochemical mechanism, the excited-state $ZnPc^{*}$ species is typically generated via bimolecular electron transfer between the reduced radical anion $ZnPc^{\bullet-}$ and the oxidized radical cation $ZnPc^{\bullet+}$ formed in the vicinity of the working electrode surface (**Equation 19**). These radical intermediates recombine to produce the electronically excited molecule, which may then emit light through radiative relaxation (**Equation 20**). However, under the experimental conditions employed, no significant ECL emission signal was detected, with intensity levels remaining negligible throughout the potential region. This lack of observable emission is likely attributable to several factors intrinsic to ZnPc: the radical species generated are inherently unstable and exhibit low reactivity, limiting the efficient formation of an emissive excited state. Furthermore, molecular aggregation, possible non-radiative decay pathways, and rapid quenching mechanisms may also contribute to the suppression of ECL emission. These observations are consistent with prior reports on phthalocyanine derivatives, where limited electrochemiluminescence response is often linked to the chemical and photophysical properties of the radical intermediates.[30-32]

Figure 7C shows the potential pulsing results involving combinations of the ZnPc dication and its four reduced species, conducted in a solution of 0.025 mM ZnPc dissolved in DMSO with 0.1 M TBAP as the supporting electrolyte. **Figure S5** presents the corresponding

data for pulsing between the radical cation and the four anionic species; however, no observable ECL emission was detected. In contrast, the pulsing combinations shown in **Figure 7C** and **Figure S6** generate measurable ECL emission, with intensities reaching up to 1 nA. Notably, **Figure S6C**, corresponding to the pulsing combination between the dication and the species generated at the fourth reduction peak, yields the highest ECL intensity in the annihilation pathway, with a maximum emission of 1.2 nA. This enhanced signal is attributed to the higher concentrations of electrogenerated radical cations and radical anions, which facilitate an increased rate of bimolecular electron transfer reactions, as outlined in **Equations 16-20**.[33]

(10) $$ZnPc \rightarrow ZnPc^{\bullet+} + e^-$$

(11) $$ZnPc^{\bullet+} \rightarrow ZnPc^{2+} + e^-$$

(12) $$ZnPc + e^- \rightarrow ZnPc^{\bullet-}$$

(13) $$ZnPc^{\bullet-} + e^- \rightarrow ZnPc^{2-}$$

(14) $$ZnPc^{2-} + e^- \rightarrow ZnPc^{\bullet 3-}$$

(15) $$ZnPc^{\bullet 3-} + e^- \rightarrow ZnPc^{4-}$$

(16) $$ZnPc^{2+} + ZnPc \rightarrow 2\ ZnPc^{\bullet+}$$

(17) $$ZnPc^{2-} + ZnPc \rightarrow 2\ ZnPc^{\bullet-}$$

(18) $$ZnPc^{\bullet 3-} + ZnPc \rightarrow ZnPc^{\bullet+} + ZnPc^{2-}$$

(19) $$ZnPc^{\bullet-} + ZnPc^{\bullet+} \rightarrow ZnPc^{*} + ZnPc$$

(20) $ZnPc^{*} \rightarrow ZnPc + h\nu$

351

352 Notably, ZnPc exhibits measurable ECL emission using the potential pulsing technique in
353 the annihilation pathway, whereas $H_2Pc(\alpha\text{-}OC_4H_9)_8$ does not. The presence of the central Zn^{2+}
354 ion is known to play a crucial role in stabilizing these radical intermediates, in contrast to the
355 metal-free centre of $H_2Pc(\alpha\text{-}OC_4H_9)_8$.[31-32] Furthermore, the bulky alkoxy substituents on $H_2Pc(\alpha\text{-}$
356 $OC_4H_9)_8$ may promote aggregation and strong intermolecular interactions, which can facilitate
357 self-quenching of excited states and an increase in nonradiative decay processes.[34] Together,
358 these structural and electronic differences likely account for the for the observable ECL in ZnPc
359 under potential pulsing annihilation conditions, while $H_2Pc(\alpha\text{-}OC_4H_9)_8$ remains effectively non-
360 emissive under similar potential pulsing annihilation conditions.

361 Furthermore, to investigate the influence of pulse duration on ECL emission, the
362 enhanced emission resulting from potential pulsing between the ZnPc dication and the species
363 formed at the fourth reduction peak was examined at varying pulsing frequencies. **Figures S7A-**
364 **D** illustrate the ECL signals of 0.025 mM ZnPc in DMSO with 0.1 M TBAP as the supporting
365 electrolyte using pulsing frequencies of 0.5 Hz, 1 Hz, 5 Hz, and 10 Hz, respectively. Notably, the
366 highest ECL intensity of 1.82 nA was observed at a frequency of 5 Hz, while frequencies of 0.5
367 Hz, 1 Hz, and 10 Hz resulted in lower maximum emissions of approximately 1.29 nA. These
368 results suggest that a pulse duration of 100 ms is optimal for the efficient generation and
369 subsequent reaction of ZnPc radical anion and radical cation species, maximizing the ECL
370 emission.

To further enhance the ECL emission of ZnPc, 5 mM of BPO was added as a coreactant. **Figure 8A** displays the CV (red) and ECL-voltage curve (blue) of 0.025 mM ZnPc in DMSO containing 5 mM BPO and 0.1 M TBAP. The ECL-voltage curve reveals multiple emission peaks, corresponding to distinct ECL processes occurring at different applied potentials.[25] A maximum ECL intensity of 344 nA was recorded, representing a 189-fold enhancement compared to the ECL observed in the annihilation pathway using a potential pulsing at a frequency of 5 Hz.

Although this is a substantial increase in ECL emission, it is less pronounced than the enhancement observed for $H_2Pc(\alpha\text{-}OC_4H_9)_8$ under similar conditions. This is likely attributed to the more favourable redox behaviour of $H_2Pc(\alpha\text{-}OC_4H_9)_8$, which generates radical ions with sufficient lifetimes and reactivity to effectively engage in electron-transfer reactions with BPO. In contrast, while the Zn^{2+} metal centre can stabilize certain electronic states it may also impose constraints on radical formation, potentially reducing orbital overlap and reaction efficiency with BPO. Additionally, the flexible coordination environment and bulky substituents of $H_2Pc(\alpha\text{-}OC_4H_9)_8$ can facilitate more efficient coreactant interactions and electron transfer, contributing to its stronger ECL signals. These factors combined may explain why $H_2Pc(\alpha\text{-}OC_4H_9)_8$ demonstrates more intense ECL emission in the coreactant pathway compared to that of the ZnPc/BPO system.

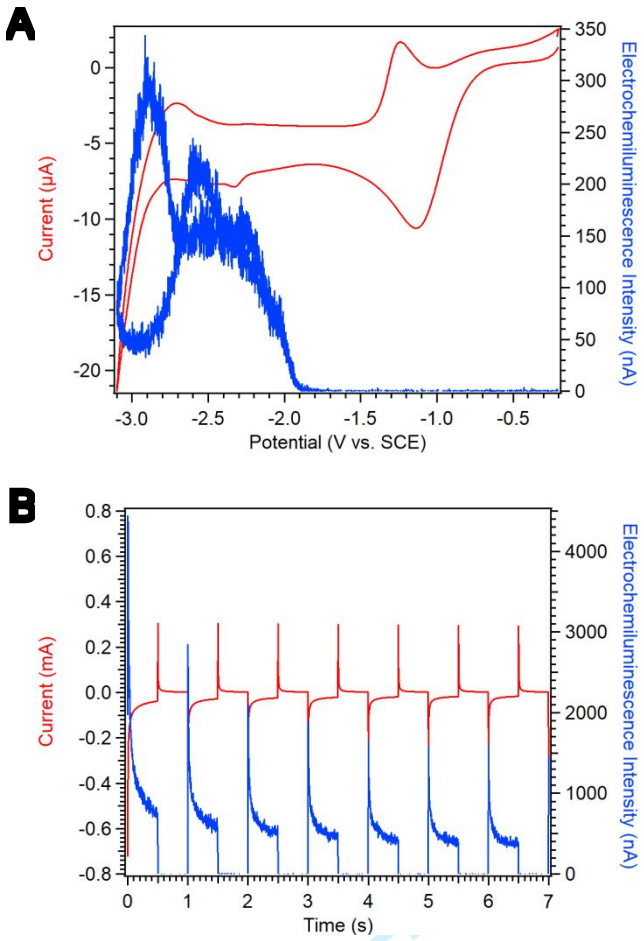

Figure 8. (A) CV (red) and ECL-voltage curve (blue) of 0.025 mM ZnPc and 5 mM BPO in DMSO with 0.1 M TBAP solution. A scan rate of 100 mV/s was utilized, cycling between −0.20 V and −3.10 V vs. SCE. (B) The current-time (red) and ECL-time (blue) curves are shown pulsing between potentials of −3.10 V and −0.20 V vs. SCE at a frequency of 1 Hz.

To further enhance the ECL emission of the ZnPc/BPO system, potential pulsing was applied across a range of frequencies. **Figure S8** show the potential pulsing of ZnPc/BPO between −3.10 V and −0.20 V vs. SCE at frequencies of 0.5 Hz (**A**), 5 Hz (**B**), and 10 Hz (**C**), and **Figure 8B** presents the potential pulsing at 1 Hz. While the ECL intensities across the different pulsing frequencies remain comparable, the highest emission was recorded at 5 Hz, reaching a maximum of 4616 nA. This result further supports the conclusion that a 100 ms pulse

duration is optimal for generating and facilitating electron transfer reactions between the ZnPc and BPO radical species, maximizing the ECL emission in coreactant conditions.

Electrochemiluminescence Spectroscopy of Unsubstituted ZnPc/BPO Coreactant System

Figure 9A shows the accumulated ECL spectrum of 0.025 mM ZnPc with 0.1 M TBAP and 5 mM BPO in DMSO obtained during a CV experiment in which the potential was cycled from −0.20 V to −3.10 V vs. SCE at a scan rate of 100 mV/s. Three peak wavelengths were observed, with the first being at 670 nm (pink), the second at 710 nm (purple), and the third at 775 nm (green). **Figure 9B** shows the photoluminescence spectra of 0.004 mM ZnPc with 0.01 M TBAP in DMSO. The solution was excited using a 532 nm laser equipped with a long-pass filter, yielding emission peaks at 670 nm, 710 nm, and 775 nm. The Q(0,0) and Q(0,1) bands correlate very well to those of previously reported fluorescence of metalated phthalocyanines.[22] The ECL emission aligns closely with that of the PL; however, the PL exhibits a greater intensity for both the 670 nm and 775 nm peaks. In addition, time-resolved measurements reported by Savolainen et al. revealed an excited singlet-state lifetime of 2.9 ± 0.2 ns for ZnPc, aligning closely with that reported previously by Kosonocky et al.[26, 35] Interestingly, the ZnPc/benzoate exciplex and ZnPc/ZnPc excimer have similar wavelengths.

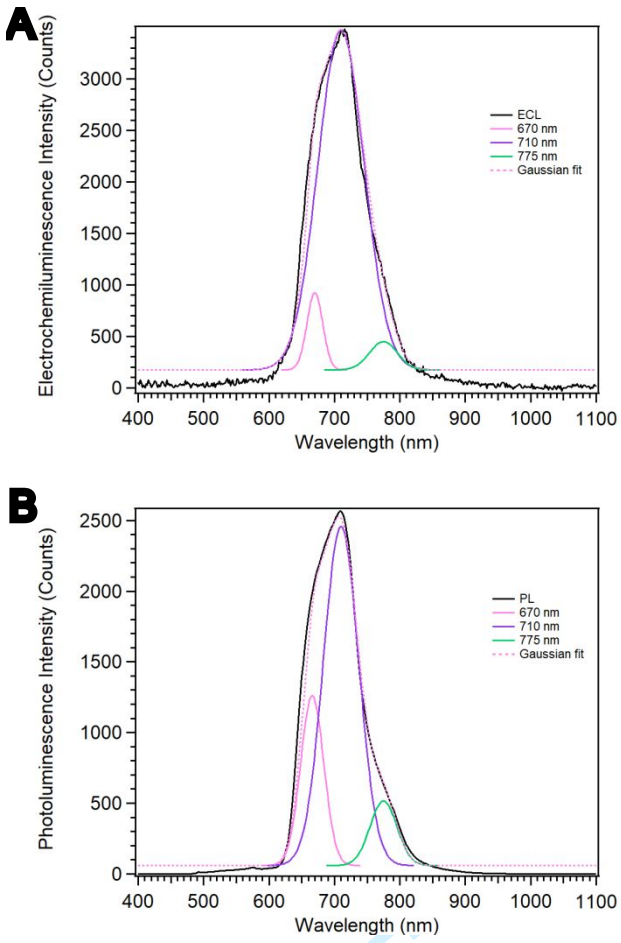

Figure 9. (A) Accumulated ECL intensity of 0.025 mM ZnPc with 5 mM BPO coreactant system during a CV scan cycling from −0.20 V to −3.10 V vs. SCE at a scan rate of 100 mV/s. (B) Photoluminescence of 0.004 mM ZnPc with 0.01 M TBAP excited by a 532 nm laser.

Figure 10A shows a three-dimensional spooling ECL spectroscopy plot obtained during a CV scan from −0.20 V to −3.10 V vs. SCE at a scan rate of 100 mV/s, with an accumulation time of 0.5 second per spectrum. The corresponding ECL intensity vs. potential profile, shown in **Figure 10B**, reveals two prominent emission maxima at −2.12 V and −2.91 V vs. SCE. These values align closely with the ECL-voltage peaks observed using the PMT, which occurred at −2.60 V and −2.91 V vs. SCE. In the cathodic scan, the evolution of ECL initiated around −1.95 V and −2.42 V vs. SCE (first and second purple peak, respectively) and began

devolving near −2.15 V vs. SCE (first purple peak). Conversely, the anodic scan illustrated the evolution of ECL at approximately −2.80 V and −2.92 V vs. SCE (first and second green peak, respectively), with devolution taking place around −3.10 V and −2.62 V vs. SCE (first and second green peak, respectively). The spooling ECL spectra provide additional insight into the nature of the excited states being produced, and how these states evolve during the ECL process. Notably, the evolution and devolution of ECL correlates well with the ECL pattern observed using the PMT. The intensity-wavelength profile exhibits variation in peak intensities, with the 710 nm peak emitting more strongly than the 670 and 775 nm peaks. As the overall emission intensity increases, the profile narrows, enhancing spectral resolution. Consequently, the 670 and 775 nm features become more distinguishable as shoulder peaks on either side of the dominant 710 nm emission. These findings align well with the parallel 5,10,15,20-tetraphenyl-21*H*, 23*H*-porphine zinc reported by Zhang et al.[20]

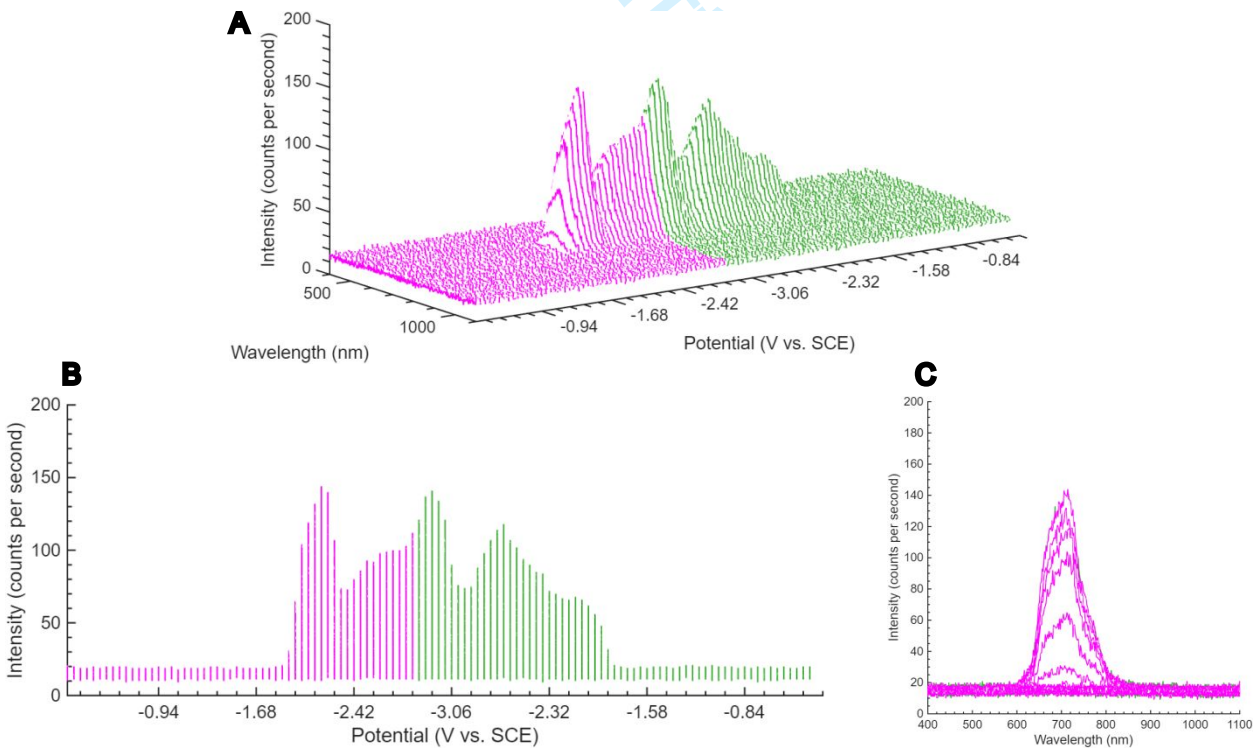

Figure 10. Spooling ECL spectra of 0.025 mM ZnPc with 5 mM BPO in DMSO during a CV experiment performed at 100 mV/s. Three views are provided, with (A) being three-dimensional, (B) being ECL intensity vs. potential, and (C) being ECL intensity vs. wavelength.

Absolute Electrochemiluminescence Quantum Efficiency of Unsubstituted ZnPc

Table 2 reports the absolute electrochemiluminescence quantum efficiency of ZnPc in coreactant conditions using BPO as the oxidative coreactant. A Φ_{ECL} value of 0.0099 ± 0.0001% was obtained by quantifying the total number of emitted photons relative to the charge passed during the ECL process. This Φ_{ECL} value, comparable to the Φ_{ECL} in the annihilation pathway of the gold standard $Ru(bpy)_3^{2+}$ and greater than the Φ_{ECL} of protoporphyrin IX dimethyl ester, a similar porphyrin derivatives,[18-19] observed for ZnPc can be attributed to the presence of the Zn^{2+} metal centre, which plays a crucial role in stabilizing radical intermediates and facilitating their reaction to form emissive excited states. Moreover, ZnPc's planar, unsubstituted structure may reduce aggregation and nonradiative losses, further supporting efficient excited-state formation. The applied potential pulsing frequency also significantly influences the absolute ECL quantum efficiency" at lower frequencies (e.g., 1 Hz), the system has more time during each pulse period for electrochemically generated species (radicals or excited states) to react and emit photons before the next pulse occurs, promoting more effective electron-transfer reactions. In contrast, at higher frequencies (e.g., 10 Hz), the pulse duration is shorter, and species required for ECL emission may not fully form, react, or emit before the potential switches again, limiting the overall ECL efficiency. These results underscore the importance of metal coordination and molecular structure in tuning the ECL performance of phthalocyanine-based emitters.

Table 2. Absolute Electrochemiluminescence Quantum Efficiency of 0.025 mM ZnPc with 5 mM BPO in a DMSO solution with 0.1 M of TBAP using various electrochemical techniques.

Technique	Absolute Electrochemiluminescence Quantum Efficiency (%)
Cyclic Voltammetry	0.0016 ± 0.0001
0.5 Hz Potential Pulsing	0.0020 ± 0.0001
1 Hz Potential Pulsing	0.0099 ± 0.0001
5 Hz Potential Pulsing	0.0012 ± 0.0001
10 Hz Potential Pulsing	0.0009 ± 0.0001

Conclusion

This study presents a comprehensive evaluation of the electrochemiluminescence behaviour and absolute quantum efficiencies of octabutoxy-substituted metal-free phthalocyanine ($H_2Pc(\alpha\text{-}OC_4H_9)_8$) and unsubstituted zinc phthalocyanine (ZnPc) under both annihilation and coreactant conditions. Notably, $H_2Pc(\alpha\text{-}OC_4H_9)_8$ exhibited minimal ECL emission in the annihilation pathway yet demonstrated a substantial enhancement when benzoyl peroxide (BPO) was added as a coreactant. Although the absolute quantum efficiency $H_2Pc(\alpha\text{-}OC_4H_9)_8$/BPO system was lower than that of similar porphyrin-based analogues, a value of 0.00075 ± 0.00003% was calculated, establishing a useful benchmark for non-metallic phthalocyanine luminophores.

Spectroscopic analysis revealed Q(0,0) and Q(0,1) transitions at 635 and 780 nm, respectively, with the formation of an exciplex at 880 nm under ECL conditions and an excimer at 900 nm observed via laser-induced photoluminescence (PL). These observations underscore

the utility of ECL spectroscopy in understanding exciplex and excimer dynamics, further corroborated by spectroelectrochemical and PL studies.

In parallel, ZnPc generated modest but observable ECL under annihilation conditions using a chronoamperometric potential-pulsing method, with an increase in emission upon introduction of BPO. The ZnPc/BPO system achieved a maximum absolute quantum efficiency of 0.0099 ± 0.0001%, which approaches that of $Ru(bpy)_3^{2+}$ in its annihilation pathway and exceeds the value previously reported for protoporphyrin IX dimethyl ester. ZnPc displayed characteristic Q(0,0) and Q(0,1) transitions at 670 and 710 nm, with the formation of an exciplex at 775 nm. Interestingly, the spectral similarity between the ZnPc/BPO exciplex and ZnPc excimer suggests closely related emissive pathways that merit further exploration.

Together, these findings highlight the tunability and mechanistic properties of phthalocyanine-based ECL systems, reinforcing the value of further studying phthalocyanines as next-generation ECL luminophores.

Acknowledgements

The generous financial support to this research from the Natural Sciences and Engineering Research Council of Canada (NSERC, DG RGPIN-2023-05337 SPG STPGP-2016-493924, and NFRFT-2020-00573), Canada Foundation for Innovation/Ontario Innovation Trust (CFI/OIT, 9040), Premier's Research Excellence Award (PREA, 2003), and The University of Western Ontario is greatly appreciated. We sincerely thank the Electronic Shop in the Department of Chemistry, Glass Shop, and Science Stores in the Faculty of Science for their quality service. We are grateful to Martin Stillman for kind consultation and discussion on phthalocyanine optical spectroscopy.

Data Availability

Data generated or analyzed during this study are available from the corresponding author upon reasonable request.

Declaration of Competing Interest

The authors declare no competing interests.

References

(1) Miao, W., 13 - Electrogenerated Chemiluminescence. In *Handbook of Electrochemistry*, Zoski, C. G., Ed. Elsevier: Amsterdam, 2007; pp 541-590.
(2) Hesari, M.; Ding, Z., Review—Electrogenerated Chemiluminescence: Light Years Ahead. *J. Electrochem. Soc.* **2016,** *163*, H3116-H3131.
(3) Zhang, C.; Cai, Z.; Chu, K.; Shiu, W.-T.; Hu, P.; Liu, L.; Zhang, Q.; Ding, Z., Exploring Surface State and Exciplex Dominated Aggregation Induced Electrochemiluminescence of Graphene Quantum Dots Prepared Via Electrochemical Exfoliation. *ChemPhysChem* **2025,** *26*, e202401074.
(4) Lee, D. S.; Zarabadi, M. P.; Bhattacharjee, H.; Qi, L.; McLeod, J. F.; Saeedfar, K.; Singh, I.; Woods, A.; Messina, A.; Birss, V. I.; Crudden, C. M.; She, Z., Toll like receptor-based electrochemical sensors via N-heterocyclic carbene-modified surfaces: towards improved sensing of DNA molecules. *Mater. Adv.* **2024,** *5*, 6063-6069.
(5) Qin, J.; Li, J.; Zeng, H.; Du, F.; Tang, D.; Tang, J., Bifunctional TiO2 Nanoflower-Induced H4TCBPE Aggregation Enhanced Electrochemiluminescence for an Ultrasensitive Assay of Organophosphorus. *Anal. Chem.* **2023,** *95*, 17903-17911.
(6) Zhou, Y.; Gao, H.; Wang, X.; Qi, H., Electrogenerated Chemiluminescence from Heteroleptic Iridium(III) Complexes with Multicolor Emission. *Inorg. Chem.* **2015,** *54*, 1446-1453.
(7) Zhou, Y.; Dong, J.; Zhao, Y.; Mao, Z., Singlet Oxygen Generation via an Electrochemical Reduction Method Assisted by a Ruthenium(II) Complex. *Inorg. Chem.* **2023,** *62*, 7155-7159.
(8) Zhang, C.; Cai, Z.; Qin, X.; Malik, F.; Zhang, Q.; Huang, J.; Zhang, R.; Ding, Z., Spectroscopic and Electrochemical Insights into Strategies Tuning Red-Green-Blue (RGB) Electrochemiluminescence from a Single Ruthenium Complex. *J. Phys. Chem. C* **2025,** *129*, 10343-10355.
(9) Wheeler, B. L.; Nagasubramanian, G.; Bard, A. J.; Schechtman, L. A.; Kenney, M. E., A silicon phthalocyanine and a silicon naphthalocyanine: synthesis, electrochemistry, and electrogenerated chemiluminescence. *J. Am. Chem. Soc.* **1984,** *106*, 7404-7410.
(10) Koca, A., Spectroelectrochemistry of Phthalocyanines. In *Electrochemistry of N4 Macrocyclic Metal Complexes: Volume 2: Biomimesis, Electroanalysis and Electrosynthesis of MN4 Metal Complexes*, Zagal, J. H.; Bedioui, F., Eds. Springer International Publishing: Cham, 2016; pp 135-200.

(11) Isago, H., Optical spectra of phthalocyanines and related compounds. *NIMS Monographs* **2015**.
(12) Hesari, M.; Ding, Z., Spooling electrochemiluminescence spectroscopy: development, applications and beyond. *Nat. Protoc.* **2021,** *16*, 2109-2130.
(13) Bae, Y.; Myung, N.; Bard, A. J., Electrochemistry and Electrogenerated Chemiluminescence of CdTe Nanoparticles. *Nano Lett.* **2004,** *4*, 1153–1161.
(14) Booker, C.; Wang, X.; Haroun, S.; Zhou, J.; Jennings, M.; Pagenkopf, B. L.; Ding, Z., Tuning of electrogenerated silole chemiluminescence. *Angew. Chem. Int. Ed.* **2008,** *47*, 7731-7735.
(15) Hesari, M.; Workentin, M. S.; Ding, Z., Thermodynamic and Kinetic Origins of Au_{25}^0 Nanocluster Electrochemiluminescence. *Chem. Eur. J.* **2014,** *20*, 15116-15121.
(16) Wei, X.; Chu, K.; Adsetts, J. R.; Li, H.; Kang, X.; Ding, Z.; Zhu, M., Nanocluster Transformation Induced by SbF6– Anions toward Boosting Photochemical Activities. *J. Am. Chem. Soc.* **2022,** *144*, 20421-20433.
(17) Adsetts, J. R.; Chu, K.; Hesari, M.; Ma, J.; Ding, Z., Absolute Electrochemiluminescence Efficiency Quantification Strategy Exemplified with $Ru(bpy)_3^{2+}$ in the Annihilation Pathway. *Anal. Chem.* **2021,** *93*, 11626-11633.
(18) Chu, K.; Adsetts, J. R.; Ma, J.; Zhang, C.; Hesari, M.; Yang, L.; Ding, Z., Physical Strategy to Determine Absolute Electrochemiluminescence Quantum Efficiencies of Coreactant Systems Using a Photon-Counting Photomultiplier Device. *J. Phys. Chem. C* **2021,** *125*, 22274-22282.
(19) Zhan, Z.; Qin, X.; Chu, K.; Sun, X.; Ding, Z., Absolute Quantum Efficiencies for Electrochemiluminescence and Chemiluminescence of Protoporphyrin IX Dimethyl Ester. *J. Electroanal. Chem.* **2023,** *932*, 117220.
(20) Zhang, R.; Zhang, A.; Stillman, M. J.; Ding, Z., Enhancement of Tetraphenylporphyrin Electrochemiluminescence by Means of Symmetry Breaking. *J. Phys. Chem. C* **2020,** *124*, 16568-16576.
(21) Ough, E. A.; Stillman, M. J., Analysis of the absorption and magnetic circular dichroism spectra of low spin (S= 1/2) iron (III) phthalocyanine. *Inorg. Chem.* **1995,** *34*, 4317-4325.
(22) Mack, J.; Stillman, M. J., Assignment of the optical spectra of metal phthalocyanines through spectral band deconvolution analysis and zindo calculations. *Coord. Chem. Rev.* **2001,** *219-221*, 993-1032.
(23) Zhang, C.; Zhang, R.; Zhang, R.; Zhang, Q.; Zhang, J.-L.; Ding, Z., Spectroscopy and absolute quantum efficiency of near-infrared electrochemiluminescence for a macrocyclic palladium complex. *J. Inorg. Biochem.* **2024,** *254*, 112514.
(24) Menzel, E. R.; Jordan, K. J., Fluorescence of solid metal-free phthalocyanine. *Chem. Phys.* **1978,** *32*, 223-229.
(25) Chu, K.; Adsetts, J. R.; Whitworth, Z.; Kumar, S.; Zysman-Colman, E.; Ding, Z., Elucidation of an Aggregate Excited State in the Electrochemiluminescence and Chemiluminescence of a Thermally Activated Delayed Fluorescence (TADF) Emitter. *Langmuir* **2023,** *39*, 2829-2837.
(26) Kosonocky, W. F.; Harrison, S. E., Saturation of Absorption and Fluorescence in Solutions of Phthalocyanines. *J. Appl. Phys.* **1966,** *37*, 4789-4797.
(27) Yang, L.; Dong, L.; Hall, D.; Hesari, M.; Olivier, Y.; Zysman-Colman, E.; Ding, Z., Insights into enhanced electrochemiluminescence of a multiresonance thermally activated delayed fluorescence molecule. *SmartMat* **2023,** *4*, e1149.

583 (28) Ishimatsu, R., Impacts of electrogenerated chemiluminescence mechanism on the
584 emission spectra and intensities. *Anal. Sci.* **2025,** *41*, 511-522.
585 (29) Yang, L.; Zhang, R.; Balónová, B.; True, A. E.; Chu, K.; Adsetts, J. R.; Zhang, C.; Qin,
586 X.; Zysman-Colman, E.; Blight, B. A.; Ding, Z., Insights into the Electrochemiluminescence
587 Process of a Hydrogen Bonding Iridium(III) Complex. *J. Electroanal. Chem.* **2022,** *920*, 116594.
588 (30) Atilla, D.; Durmuş, M.; Gürek, A. G.; Ahsen, V.; Nyokong, T., Synthesis, photophysical
589 and photochemical properties of poly (oxyethylene)-substituted zinc phthalocyanines. *Dalton*
590 *Trans.* **2007**, 1235-1243.
591 (31) Castro, K. A. D. F.; Prandini, J. A.; Biazzotto, J. C.; Tomé, J. P. C.; da Silva, R. S.;
592 Lourenço, L. M. O., The Surprisingly Positive Effect of Zinc-Phthalocyanines With High
593 Photodynamic Therapy Efficacy of Melanoma Cancer. *Front. Chem.* **2022,** *10*.
594 (32) Potlog, T.; Lungu, I.; Tiuleanu, P.; Robu, S., Photophysical Properties of Linked Zinc
595 Phthalocyanine to Acryloyl Chloride:N-vinylpyrrolidone Copolymer. *Polymers (Basel)* **2021,** *13*,
596 4428.
597 (33) Shen, M.; Rodríguez-López, J.; Huang, J.; Liu, Q.; Zhu, X.-H.; Bard, A. J.,
598 Electrochemistry and Electrogenerated Chemiluminescence of Dithienylbenzothiadiazole
599 Derivative. Differential Reactivity of Donor and Acceptor Groups and Simulations of Radical
600 Cation−Anion and Dication−Radical Anion Annihilations. *J. Am. Chem. Soc.* **2010,** *132*, 13453-
601 13461.
602 (34) Aarabi, M.; Aranda, D.; Gholami, S.; Meena, S. K.; Lerouge, F.; Bretonniere, Y.; Gürol,
603 I.; Baldeck, P.; Parola, S.; Dumoulin, F.; Cerezo, J.; Garavelli, M.; Santoro, F.; Rivalta, I.,
604 Quantum-Classical Protocol for Efficient Characterization of Absorption Lineshape and
605 Fluorescence Quenching upon Aggregation: The Case of Zinc Phthalocyanine Dyes. *J. Chem.*
606 *Theory Comput.* **2023,** *19*, 5938-5957.
607 (35) Savolainen, J.; van der Linden, D.; Dijkhuizen, N.; Herek, J. L., Characterizing the
608 functional dynamics of zinc phthalocyanine from femtoseconds to nanoseconds. *J. Photochem.*
609 *Photobiol. A: Chem.* **2008,** *196*, 99-105.

610